Observations of Local Positive Low Cloud Feedback Patterns, and Their Role in Internal Variability and Climate Sensitivity

Tianle Yuan[1,2,*], Lazaros Oreopoulos[2], Steven Platnick[2], Kerry Meyer[2]

[1]Joint Center for Earth Systems Technology, University of Maryland, Baltimore County, Baltimore, MD, 21228
[2]Earth Sciences Division, NASA Goddard Space Flight Center, Greenbelt, MD, 20771

Abstract

Modeling studies have shown that cloud feedbacks are sensitive to the spatial pattern of sea surface temperature (SST) anomalies, while cloud feedbacks themselves strongly influence the magnitude of SST anomalies. Observational counterparts to such patterned interactions are still needed. Here we show that distinct large-scale patterns of SST and low-cloud cover (LCC) emerge naturally from objective analyses of observations and demonstrate their close coupling in a positive local SST-LCC feedback loop that may be important for both internal variability and climate change. The two patterns that explain the maximum amount of covariance between SST and LCC correspond to the Interdecadal Pacific Oscillation (IPO) and the Atlantic Multidecadal Oscillation (AMO), leading modes of multidecadal internal variability. Spatial patterns and time series of SST and LCC anomalies associated with both modes point to a strong positive local SST-LCC feedback. In many current climate models, our analyses suggest that SST-LCC feedback strength is too weak compared to observations. Modeled local SST-LCC feedback strength affects simulated internal variability so that stronger feedback produces more intense and more realistic patterns of internal variability. To the extent that the physics of the local positive SST-LCC feedback inferred from observed climate variability applies to future greenhouse warming, we anticipate significant amount of delayed warming because of SST-LCC feedback when anthropogenic SST warming eventually overwhelm the effects of internal variability that may mute anthropogenic warming over parts of the ocean. We postulate that many climate models may be underestimating both future warming and the magnitude of modeled internal variability because of their weak SST-LCC feedback.

1. Introduction

Global scale climate change can be described in an energy balance framework[*Gregory et al.*, 2002]: $F(t) = N(t) + \alpha(t)T(t) + \varepsilon$. Radiative forcing, $F(t)$, imposed on the climate system is balanced by the sum of net downward radiative flux, $N(t)$, radiative response $\alpha(t)T(t)$, and a small residual ε. $\alpha(t)$, the time-dependent climate feedback parameter, measures the global radiative response per degree of surface air temperature T change. Its reciprocal $\lambda(t) = {}^{1}/_{\alpha(t)}$, called the climate sensitivity parameter, measures the warming per unit increase in radiative forcing [*Gregory and Andrews*, 2016]. Assuming $\alpha(t)$to be constant, equilibrium climate sensitivity can be estimated by quantifying changes in temperature (ΔT), ocean heat uptake (excellent proxy for ΔN) and radiative forcing (ΔF) over a period according to $\lambda_{eq} = {}^{\Delta T}/_{(\Delta F - \Delta N)}$.

In the instrumental record, the global mean warming rate, ${}^{\Delta T}/_{\Delta t}$, is not constant and undergoes periods of acceleration and deceleration (Figure 1A) [Morice et al., 2012; Hansen et al., 2010]. The warming rate is also spatially heterogeneous with characteristic large-scale patterns (Figures 1B and 1C). Both internal variability and changing ($F(t)$) can make ${}^{\Delta T}/_{\Delta t}$ and warming patterns change with time (Figures 1B and 1C). Model analyses suggest that time-varying patterns of sea surface temperature (SST) can actively change $\alpha(t)$, and therefore${}^{\Delta T}/_{\Delta t}$, by convolving with individual feedback processes [*Held et al.*, 2010; *Armour et al.*, 2013; *Andrews et al.*, 2015]. The low cloud feedback plays a critical role in this process [*Andrews et al.*, 2012; *Rose et al.*, 2014; *Andrews et al.*, 2015; *Gregory and Andrews*, 2016; *Zhou et al.*, 2016]. It is perhaps best illustrated in an idealized model experiment where simply changing the SST pattern, without altering the global mean T, produces a nonzero $N(t)$ due to cloud anomalies [*Andrews et al.*, 2015; *Zhou et al.*, 2016]. Recent modeling studies also show that observed time-varying patterns of SST in recent decades have significantly changed $\alpha(t)$ [*Gregory and Andrews*, 2016; *Zhou et al.*, 2016; *Marvel et al.*, 2018]. Low cloud feedback can in turn affect modeled SST internal variability[*Zhang et al.*, 2010; *Brown et al.*, 2014; *Bellomo et al.*, 2014b; *Myers et al.*, 2017]. However, direct observational evidence of patterned coupling between SST and low clouds are needed.

Here we examine large-scale patterns of low-cloud cover (LCC) and SST and their coupling at near-global scales (60°S ~60°N) using satellite data and compare them with patterns produced by global climate models. LCC feedback is a major component of the overall cloud feedback [*Clement et al.*, 2009] [*Qu et al.*, 2014; *Zelinka et al.*, 2016]. Previous regression analyses have shown that SST exerts a prime control on local and regional mean LCC variations, with inversion strength, a proxy for lower troposphere stability, being the next most important factor [*Qu et al.*, 2014; *Brient and Schneider*, 2016]. Patterns of large-scale LCC variability at interannual and longer time scales and their coupling with SST have received less attention, however. Here we focus on large-scale spatial patterns and associated temporal variations. The LCC-SST feedback analyzed here is assumed to encompass both the direct influence of SST on LCC as well as the indirect meteorological influences (e.g., stability) that vary in concert with SST. Our analysis does not separate out the remote impact of SST anomaly on LCC through modifying troposphere stability in remote areas [Qu et al., 2014; Zhou et al., 2017].

2. Data and analysis methods

2.1 Data sets

We use the bias corrected International Satellite Cloud Climatology Project (ISCCP) cloud fraction data [*Norris and Evan*, 2015]. Artifacts removed include those associated with changes in viewing geometry, satellite transitions, and other factors. The process for removing spurious variability also removes any real variability occurring in the $60^oS \sim 60^oN$, but has little impact on investigations of regional changes examined in this study. Here the sum of low and mid-level cloud fraction is used to better represent the true total low cloud fraction [*Yuan et al.*, 2016]. Aqua MODIS level-3 monthly products are also used to derive low cloud fraction [*Platnick et al.*, 2016]. MODIS onboard Aqua is well calibrated. Specifically, we divide the total number of pixels whose cloud top pressure is higher than 680hPa by the total number of pixels in a grid. We compare the climatology of MODIS and ISCCP LCC using these definitions and their spatial patterns are broadly similar with each other, with noticeable differences in places such as tropical Eastern Pacific (see Fig S1).

We use CRUTEM4 [*Smith et al.*, 2008] for surface air temperature and Extended Reconstructed Sea Surface Temperature (ERSST) from the NOAA Climatic Data Center[*Dee et al.*, 2011] for SST data. Meteorological variables from ECMWF Re-analysis (ERA) interim (ERA-Interim) is used to derive the estimated inversion strength (EIS) [*Wood and Bretherton*, 2006].

2.2 Methods

We apply maximum covariance analysis (MCA) [*Bretherton et al.*, 1992] and empirical orthogonal function (EOF) analysis to objectively obtain patterns naturally emerging from observations and their time series. MCA performs a singular value decomposition of the covariance matrix between two different variables. The spatial patterns of each variable are the singular vectors, and the temporal variability is obtained by projecting the spatial patterns back onto the original data fields. The leading modes of MCA maximize the covariance between the two variables. The method identifies modes (with spatial patterns and temporal variability) that both dominate the variability in the two variables and are potentially strongly correlated with one another. The correlation coefficients between expansion coefficients, i.e. the temporal variability of corresponding spatial patterns, indicate how tightly the two are related. EOF performed on individual data sets finds dominant patterns that explain the most variance and their time series by projecting each pattern back onto the original data. Here we present spatial patterns of each mode by regressing its time series, after normalization, onto the original data set. Each grid value in the pattern quantifies the amount of change in this variable associated with one standard deviation of change in the time series.

We address the challenge of interpreting decadal changes of LCC by examining two independent global satellite data records and analyzing characteristic patterns instead of local or regional trends i.e. the bias-corrected monthly mean gridded ISCCP LCC between 1984 and 2009 and the Aqua MODIS LCC between 2003-2015. Seasonal cycle of LCC is removed. Concurrent EIS and SST are also brought into the fold to illustrate their accompanying changes.

3. Results

The leading MCA mode corresponds to the Interdecadal Pacific Oscillation (IPO) [*Power et al.*, 1999] and its SST and LCC patterns consistently suggest a positive LCC-SST feedback across different oceans. In the leading SST pattern (Figure 2A), the largest SST anomalies are found in the tropical East Pacific cold tongue region and they are flanked by two middle latitude anomalies of opposite sign in both hemispheres to the west. SST anomalies along west coasts of the Americas have the same sign as the tropical peak. This pattern can also be roughly discerned in Figures 1B and 1C. The corresponding pattern of LCC nearly mirrors that of the SST mode, only with reversed sign (Figure 2B): Areas with negative SST anomalies are associated with positive LCC anomalies, which suggests a positive SST-LCC feedback: the effect of reduced LCC has a warming effect and reinforces positive SST anomalies. For example, LCC in the Eastern Tropical Pacific strongly increases when a La Nina-like, cool SST anomaly dominates. Concurrent negative SST anomalies in the Californian and Peruvian stratocumulus regions, to the north and south of tropical anomalies, are accompanied by LCC increase. Meanwhile, LCC decreases in areas where warm SST anomalies prevail in the southern and northern flanks of the tropical cold anomalies. This MCA mode explains 50% of the interannual covariance between SST and ISCCP LCC.

The second MCA mode corresponds to the Atlantic Multidecadal Oscillation (AMO) [*Enfield and Nuñez*, 2001], the dominant multidecadal variability in the Atlantic Basin, and its SST and LCC patterns also suggest a positive LCC feedback. The SST pattern of the second MCA mode (Figure 2D) has strong anomalies in both the Pacific and the Atlantic Oceans. In the North Atlantic, the anomalies form a horseshoe pattern with two arms, one in the middle latitudes and another in the tropical Atlantic [Figure 2D], which is a characteristic of the AMO. Large positive SST anomalies are found in the Eastern Pacific and in the North Pacific. The Eastern Pacific anomalies are much more spatially confined than those of a typical ENSO signal, while the North Pacific anomalies are quite similar to the Pacific Decadal Oscillation[*Deser et al.*, 2004]. The overall Pacific pattern is strikingly similar to the modeled pattern that represents the impact of AMO on the Pacific [*Zhang and Delworth*, 2007; *Li et al.*, 2016]. The corresponding LCC pattern [Figure 2E] is nearly identical to the pattern produced by regressing LCC onto the AMO index in the Atlantic [*Yuan et al.*, 2016]. Positive LCC anomalies are again found over regions with negative SST anomalies. In the Pacific, the same negative coupling (i.e. positive feedback) between SST and LCC anomalies exists. For example, positive LCC anomalies are found over cold tropical Eastern Pacific SST anomalies; similar negative coupling is observed for LCC and SST anomalies in the North Pacific, which again suggests a positive LCC-SST feedback. This MCA mode explains 19% of the covariance. It should be emphasized that both patterns emerge naturally from the objective analysis method and they resemble known modes (IPO and AMO) of coupled internal variability. The emergence of such congruent and physically meaningful SST and LCC patterns from observations suggest a physical underpinning.

Our new observational evidence of the systematic large-scale patterns of positive SST-LCC feedback is consistent with both theoretical [e.g. summarized in [*Bretherton*, 2015]and previous empirical evidence [*Qu et al.*, 2014; 2015; *Brient and Schneider*, 2016]. Physically, an increase in SST tends to decrease the inversion strength, promote mixing of dry and warm free-troposphere air into the cloudy layer, and therefore reduce cloud fraction. Regression analyses show SST often exerts the primary control on LCC in current climate [*Qu et al.*, 2014; *Brient and Schneider*, 2016]. The patterns of cloud change and its connection with SST are also

physically consistent with variations in estimated inversion strength (EIS) as shown in Figure 2F. The leading pattern of EIS has excellent agreement with those from SST and LCC in both datasets, which suggests an SST-driven local stability response in which warm SST anomalies reduce EIS.

Additional analysis further confirms the presence of a positive SST-LCC feedback that spans the decadal time scale and has coherent spatial structures. For example, expansion coefficients of both patterns of LCC and SST are significantly correlated with each other (r = 0.92 for the first mode, and r = 0.7 for the second). They are also highly correlated with indices of IPO [*Power et al.*, 1999] (r= 0.98 and r= -0.89 for the first mode of SST and LCC, respectively) and AMO [*Enfield and Nuñez*, 2001] (r = 0.83 and r=-0.59 for the second mode of SST and LCC, respectively). These results reaffirm the similarity in spatial patterns and prove the link between SST and LCC patterns in the time dimension (Figure 3). Analysis of Aqua MODIS LCC data during 2003~2015 gives independent support to SST-LCC feedback. MODIS data coverage is shorter, and its patterns may have stronger signals of higher frequency variability. Nevertheless, when applying the same procedure, patterns of leading modes of SST and MODIS LCC are also found to be negatively correlated, and their spatial patterns and temporal variability are closely related to IPO (mode 1), r = 0.78, and AMO, r = 0.62, (mode 3) indices, broadly similar to ISCCP LCC [Figure 2C] with notable differences at a few areas. This is significant because sampling, sensor characteristics, and algorithms used for MODIS and ISCCP are all different, and they cover different periods. The consistent and emergent results from independent data suggest a robust patterned SST-LCC coupling. Similar patterns also emerge from EOF analysis performed on individual fields which reveal that their principal components are strongly correlated with each other. The fact that EOF analysis corroborates the MCA analysis suggests that these patterns and their relationships are robust.

We evaluate how skillful models are in simulating LCC response to SST by applying similar analyses to cloud data from 10 models that have run atmospheric model intercomparison project (AMIP) experiments, where each model is driven by observed boundary conditions such as SST and sea ice concentration accompanied by best-estimate concentrations of forcing agents [*TAYLOR et al.*, 2012]. An ISCCP simulator [*Klein and Jakob*, 1999; *Webb et al.*, 2001]was applied to model cloud data to facilitate a more meaningful observation-model comparison. To simplify the analysis, we regress both observed and modeled cloud data against IPO and AMO monthly indices, which can be taken as less strict test for the models since it does not require the model to correctly model the covariance structure between SST and modeled LCC. Models are rather skillful at capturing the overall pattern of SST-LCC coupling as pattern correlation coefficients between modeled and observed regression patterns are above 0.44 (see Table S1) for IPO. However, the strength of SST-LCC coupling, measured by percent change in LCC per degree of SST change, exhibits large variations across different models with the majority being too weak in the critical subtropical low cloud regions (see Figures S5 and S6 and Tables S1 and S2). HadGem2-ES is one of the best performing models with pattern correlation coefficients among the highest for both modes of variability and regression values between SST and LCC for both Pacific and Atlantic basins (Figs. 4A, 4B and S2) that are closest to the observed values in high LCC regions (Figure 4A and B and Tables S1 and S2).

Our observational analysis shows that large-scale SST anomaly patterns introduced by coupled atmosphere-ocean internal variability are amplified by a robust SST-LCC feedback. Simulated SST-LCC feedback strength, in turn, has been shown to affect the amplitude of SST internal variability in models [*Bellomo et al.*, 2014a; *Brown et al.*, 2016; *Myers et al.*, 2017]. We test the effect of feedback strength on modeled internal SST amplitude by contrasting models with strong and weak SST-LCC feedback magnitude. First, we select two regions that are dominated by low level clouds, one off Californian coast and the other in the tropical North Atlantic as indicated by the red boxes in Figure 4 {Klein:1993vk}. The latitudinal and longitudinal boundaries for the two boxes are 10N to 30N and 100W to 120W, and 5N to 25N and 25W to 45W. We then regress detrended AMIP LCC anomalies against detrended observed SST anomalies and pick three models with the highest regression slopes and three with the lowest. This AMIP-based calculation selects models that have strong and weak LCC responses to SST. For both groups of models, we calculate detrended SST anomalies at each oceanic grid point and regress it against box mean SST anomalies in respectively regions, which is used a measure of the internal variability[*Bellomo et al.*, 2014a][*Myers et al.*, 2017]. We then use CMIP5 historical simulations of coupled version of each selected model to highlight the potential effect of SST-LCC on coupled simulations. Since we normalize the box mean SST anomaly time series, regression slopes for each grid point are SST anomaly amplitude associated with one standard deviation of box-mean SST anomalies. These amplitudes represent amplitude of internal SST variability linearly associated with the variability in the boxed region, which has been used as a proxy for amplitude of internal SST variability [Myers et al., 2017]. We plot the three-model mean in Figure 4. Global maps of these quantities can be seen in Fig S4.

The amplitudes of internal SST variability at interannual time scales in models with high SST-LCC feedback magnitude are nearly twice as large in Coupled Model Intercomparison Project Phase 5 (CMIP5) coupled historical simulations in both the Pacific and Atlantic (Figure 4C to F and Figures S3 and S4). Their SST regression patterns (Fig S4) are also more realistic when compared to observed patterns (Fig S3. The critical role of low cloud feedback in modulating the amplitude and persistence of internal variability is supported by recent studies [*Zhang et al.*, 2010; *Brown et al.*, 2014; *Bellomo et al.*, 2014b; *Myers et al.*, 2017]. Improving the overall SST-LCC coupling, which includes both the direct SST influence and co-varying meteorological influences, is therefore important in order for models to simulate internal variability better.

4. Summary and Discussion: Relevance to future warming

Results here give new observational support to positive SST-LCC feedback with characteristic spatial patterns that can be decomposed into familiar IPO and AMO modes. Current models can capture the IPO SST-LCC coupling pattern rather well, but their feedback magnitudes are weaker than those inferred from observations. The SST-LCC feedback strength as measured by the regression slope between them is important in determining model simulated magnitude and patterns of internal variability. Models with stronger SST-LCC feedback tend to have better representation of internal variability patterns and larger amplitudes. The patterned coupling between SST and LCC fields may serve as a holistic constraint for model evaluation.

Similar physics will operate in the global warming context with regard to SST-LCC feedback. Analyses of CO2 quadrupling experiments have demonstrated that implied climate sensitivity

generally increases with time. It happens when forced SST warming eventually overwhelms SST cooling due to internal variability or ocean heat uptake in the upwelling regions, which gets further amplified by positive cloud feedback [*Andrews et al.*, 2015]. We refer this warming as latent warming here. Intriguingly, the spatial pattern of additional cloud feedback that drives the latent warming (Figs 4 and 5 in [*Andrews et al.*, 2015]), i.e. the delayed warming that is amplified by cloud feedbacks, matches the leading LCC pattern reported here (Figure 2B). This pattern also bears resemblance to the slow warming pattern in the Pacific from another state-of-the-art model [*Held et al.*, 2010]. Our observational analysis when considered together with these modeling results imply stronger latent warming and possibly higher climate sensitivity than current estimates for many models because the SST-LCC feedback of current models is too weak. SST-LCC feedback being too weak in many models suggests that a higher equilibrium climate sensitivity might be more realistic (see [*Klein et al.*, 2017] and references therein). Indeed, we find that models capturing better the SST-LCC coupling, as measured by the spatial correlation, have higher values of equilibrium climate sensitivity (Figure S7), which may be a result of both stronger overall positive cloud feedback and stronger latent warming. For example, HadGEM2-ES, the best overall performing model using our metric, has one of the highest climate sensitivities and strong latent warming[*Andrews et al.*, 2015].

Figures

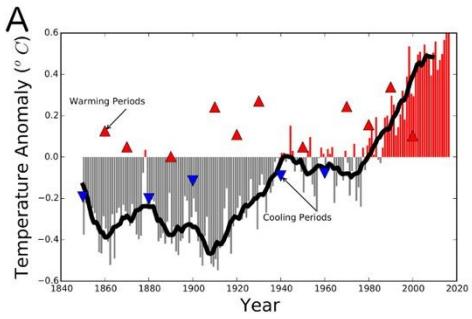

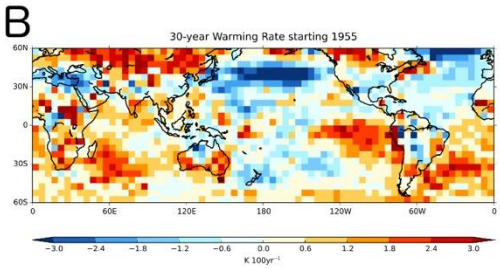

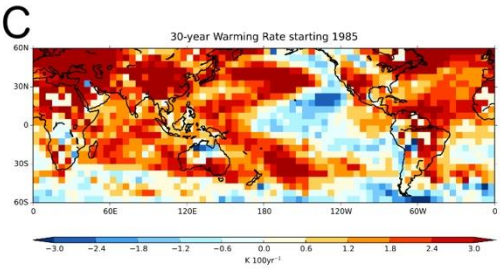

Figure 1: A) HadCRUT4 global mean surface temperature time series with a 10-year smoothing applied. For each decade, a 15-year trend is calculated. Red triangles correspond to warming trends and blue triangles to cooling trends. B) map of local surface temperature trends between1960 and 1990. C) the same as b, but for 1985-2015.

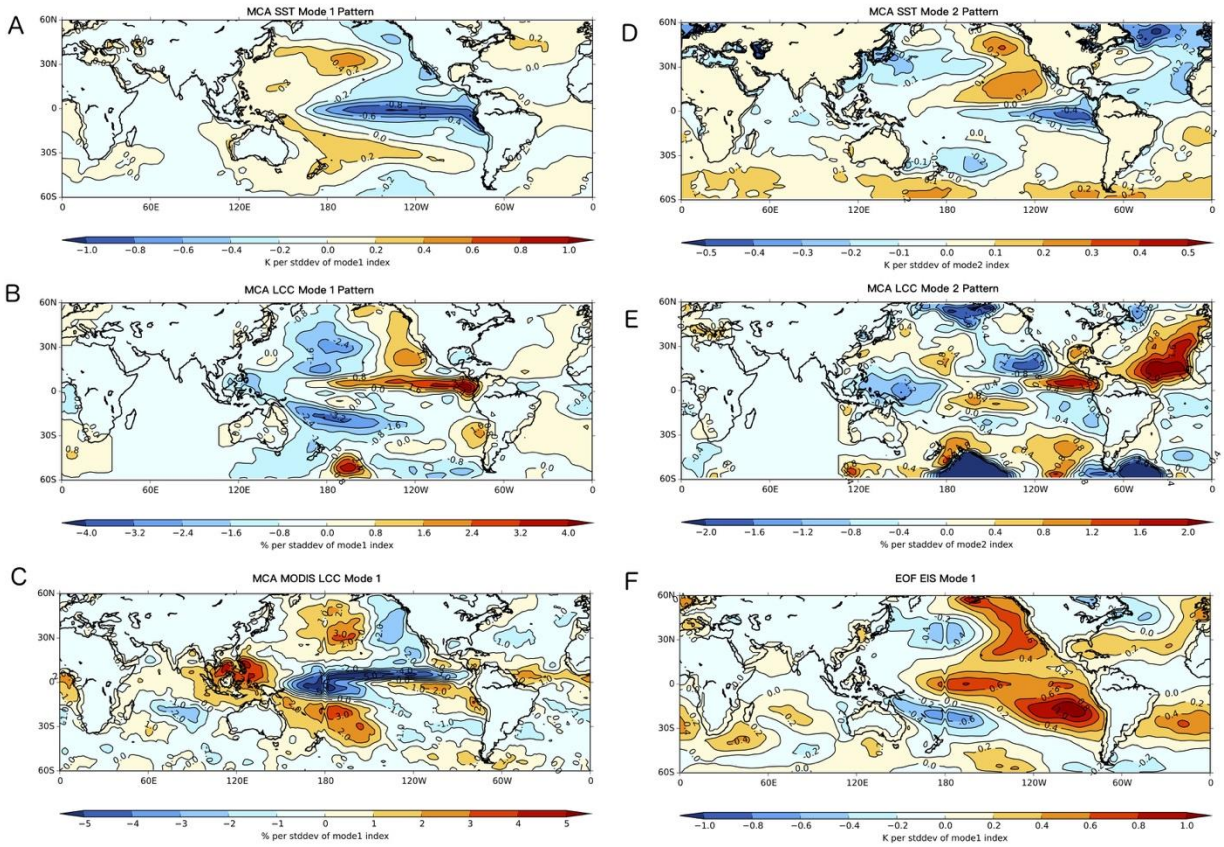

Figure 2: A) and D) SST anomalies corresponding to one standard deviation of expansion coefficients from MCA analysis, representing IPO and AMO for the period 1984-2009. B) and E) the same for LCC using ISCCP data. C) the same for IPO mode of LCC using MODIS data. F) the same for estimated inversion strength (EIS) using ERA-Interim during 1984 and 2009 for the IPO mode. In A, B, D and E, the area with longitudes between 30E and 110 E is masked out because the lack of geostationary satellite data makes the ISCCP LCC variance meaningless.

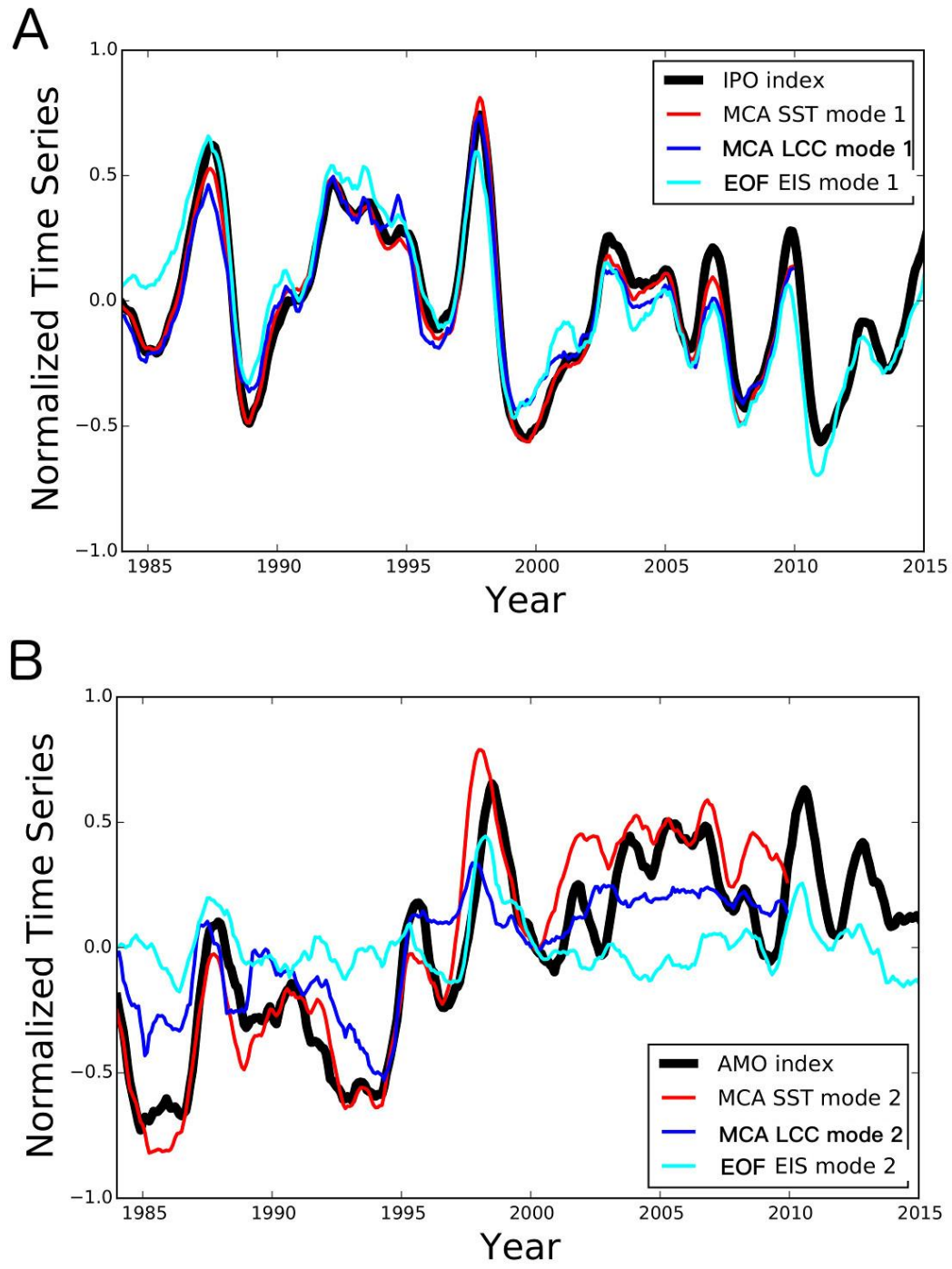

Figure 3: A) IPO index (black) between 1984 and 2015 plotted alongside time series of the first MCA mode indices for LCC (blue), SST (red), and the first EOF of estimated inversion strength (inverted, cyan). A 12-month moving average is applied to all indices. B) Similar to (A), but for AMO index and the second MCA/EOF modes.

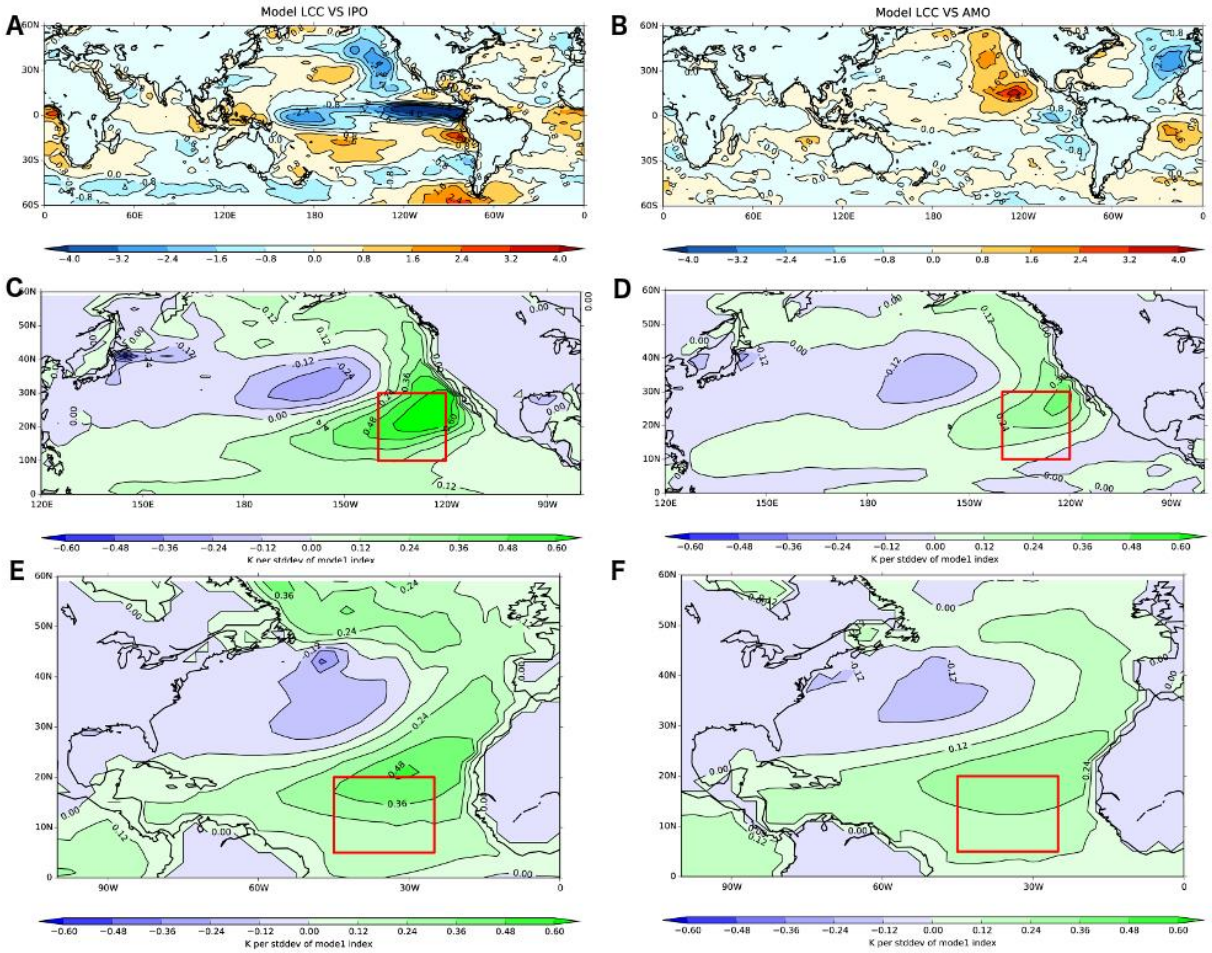

Figure 4: A) and B) regression patterns of LCC onto IPO and AMO, respectively, for the HadGEM2-ES AMIP simulation. We compare the amplitude of internal variability of SST in coupled historical simulations as defined in the text for models that have the highest (C and E) and lowest (D and F) SST-LCC feedback strength in AMIP simulations.

Allen, RJ, R. Bennartz, and D. J. Vimont (2013), The Modification of Sea Surface Temperature Anomaly Linear Damping Time Scales by Stratocumulus Clouds, *J Climate*, *26*(11), 3619–3630, doi:10.1175/JCLI-D-12-00370.1.

Andrews, T., J. M. Gregory, and M. J. Webb (2012), Forcing, feedbacks and climate sensitivity in CMIP5 coupled atmosphere- ocean climate models, *Geophy. Res. Lett.*

Andrews, T., J. M. Gregory, and M. J. Webb (2015), The Dependence of Radiative Forcing and Feedback on Evolving Patterns of Surface Temperature Change in Climate Models, *J Climate*, *28*(4), 1630–1648, doi:10.1175/JCLI-D-14-00545.1.

Armour, K. C., C. M. Bitz, and G. H. Roe (2013), Time-varying climate sensitivity from regional feedbacks, *J Climate*.

Bellomo, K., A. C. Clement, and J. R. Norris (2014a), Observational and model estimates of cloud amount feedback over the Indian and Pacific Oceans, *Journal of …*.

Bellomo, K., A. Clement, T. Mauritsen, and G. Radel (2014b), Simulating the role of subtropical stratocumulus clouds in driving Pacific climate variability, *Journal of …*.

Bretherton, C. S. (2015), Insights into low-latitude cloud feedbacks from high-resolution models, *Phil Trans R Soc A*.

Bretherton, C. S., C. Smith, and J. M. Wallace (1992), An intercomparison of methods for finding coupled patterns in climate data, *J Climate*.

Brient, F., and T. Schneider (2016), Constraints on climate sensitivity from space-based measurements of low-cloud reflection, *J Climate*.

Broccoli, A. J., and S. A. Klein (2010), Comment on “Observational and model evidence for positive low-level cloud feedback,” *Science*.

Brown, P. T., M. S. Lozier, and R. ZHANG (2016), The necessity of cloud feedback for a basin- scale Atlantic Multidecadal Oscillation, *Geophy. Res. Lett.*

Brown, P. T., W. Li, L. Li, and Y. Ming (2014), Top- of- atmosphere radiative contribution to unforced decadal global temperature variability in climate models, *Geophys Res Lett*.

Clement, A. C., R. Burgman, and J. R. Norris (2009), Observational and Model Evidence for Positive Low-Level Cloud Feedback, *Science*, *325*(5939), 460–464, doi:10.1126/science.1171255.

Dee, D. P., S. M. Uppala, and A. J. Simmons (2011), The ERA- Interim reanalysis: Configuration and performance of the data assimilation system, *Quarterly Journal of …*.

Deser, C., A. S. Phillips, and J. W. Hurrell (2004), Pacific interdecadal climate variability: Linkages between the tropics and the North Pacific during boreal winter since 1900, *J Climate*.

Enfield, D. B., and A. M. Nuñez (2001), The Atlantic multidecadal oscillation and its relation to rainfall and river flows in the continental US, *Geophy. Res. Lett.*

Gregory, J. M., and T. Andrews (2016), Variation in climate sensitivity and feedback parameters during the historical period, *Geophys Res Lett*, *43*(8), 3911–3920, doi:10.1002/2016GL068406.

Gregory, J. M., R. J. Stouffer, S. C. B. Raper, P. A. Stott, and N. A. Rayner (2002), An Observationally Based Estimate of the Climate Sensitivity, *J Climate*, *15*(22), 3117–3121, doi:10.1175/1520-0442(2002)015<3117:AOBEOT>2.0.CO;2.

Hansen, James, Reto Ruedy, Mki Sato, and Ken Lo. "Global surface temperature change." *Reviews of Geophysics* 48, no. 4 (2010).

Held, I. M., M. Winton, K. Takahashi, and T. Delworth (2010), Probing the fast and slow components of global warming by returning abruptly to preindustrial forcing, *… of Climate*.

Henley, B. J., J. Gergis, D. J. Karoly, S. Power, and J. Kennedy (2015), A tripole index for the interdecadal Pacific oscillation, *Clim Dynam*.

Jones, P. D., D. H. Lister, and T. J. Osborn (2012), Hemispheric and large- scale land-surface air temperature variations: An extensive revision and an update to 2010, *Journal of …*.

Klein, S. A., and D. L. Hartmann (1993), The Seasonal Cycle of Low Stratiform Clouds, *J Climate*, *6*(8), 1587–1606, doi:10.1175/1520-0442(1993)006<1587:TSCOLS>2.0.CO;2.

Klein, S. A., A. Hall, J. R. Norris, and R. Pincus (2017), Low-Cloud Feedbacks from Cloud-Controlling Factors: A Review, *Surveys in Geophysics*, *38*(6), 1307–1329, doi:10.1007/s10712-017-9433-3.

Klein, S. A., and C. Jakob (1999), Validation and Sensitivities of Frontal Clouds Simulated by the ECMWF Model, *Mon Weather Rev*, *127*(10), 2514–2531, doi:10.1175/1520-0493(1999)127<2514:VASOFC>2.0.CO;2.

Li, X., S.-P. Xie, S. T. Gille, and C. Yoo (2016), Atlantic-induced pan-tropical climate change over the past three decades, *Nature Climate Change*, *6*(3), 275–279, doi:doi:10.1038/nclimate2840.

Marvel, K., R. Pincus, G. A. Schmidt, and R. L. Miller (2018), Internal Variability and Disequilibrium Confound Estimates of Climate Sensitivity From Observations, *Geophys Res Lett*, *45*(3), 1595–1601, doi:10.1002/2017GL076468.

Morice, Colin P., John J. Kennedy, Nick A. Rayner, and Phil D. Jones. "Quantifying uncertainties in global and regional temperature change using an ensemble of observational estimates: The HadCRUT4 data set." *Journal of Geophysical Research: Atmospheres* 117, no. D8 (2012).

Myers, T. A., C. R. Mechoso, and M. J. DeFlorio (2017), Coupling between marine boundary layer clouds and summer-to-summer sea surface temperature variability over the North Atlantic and Pacific, *Clim Dynam*, doi:10.1007/s00382-017-3651-8.

Norris, J. R., and A. T. Evan (2015), Empirical removal of artifacts from the ISCCP and PATMOS-x satellite cloud records, *Journal of Atmospheric and Oceanic …*.

Platnick, S., K. G. Meyer, M. D. King, and G. Wind (2016), The MODIS Cloud Optical and Microphysical Products: Collection 6 Updates and Examples From Terra and Aqua, *… on Geoscience and …*.

Power, S., T. Casey, C. Folland, A. Colman, and V. Mehta (1999), Inter-decadal modulation of the impact of ENSO on Australia, *Clim Dynam*.

Qu, X., A. Hall, and S. A. Klein (2015), Positive tropical marine low- cloud cover feedback inferred from cloud- controlling factors, *Geophy. Res. Lett.*

Qu, X., A. Hall, S. A. Klein, and P. M. Caldwell (2014), On the spread of changes in marine low cloud cover in climate model simulations of the 21st century, *Clim Dynam*.

Rienecker, M. M. et al. (2011), MERRA: NASA's Modern-Era Retrospective Analysis for Research and Applications, *J Climate*, *24*(14), 3624–3648, doi:10.1175/JCLI-D-11-00015.1.

Rose, B., K. C. Armour, and D. S. Battisti (2014), The dependence of transient climate sensitivity and radiative feedbacks on the spatial pattern of ocean heat uptake, *Geoph. Res. Lett.*

Rossow, W. B., and R. A. Schiffer (1999), Advances in understanding clouds from ISCCP, *B Am Meteorol Soc*, *80*(11), 2261–2287.

Smith, T. M., R. W. Reynolds, and T. C. Peterson (2008), Improvements to NOAA's historical merged land-ocean surface temperature analysis (1880-2006), *Journal of …*.

TAYLOR, K. E., R. J. Stouffer, and G. A. Meehl (2012), *An overview of CMIP5 and the experiment design, B. Am. Meteorol. Soc., 93, 485--498, doi: 10.1175*.

Webb, M., C. Senior, S. Bony, and J. J. MORCRETTE (2001), Combining ERBE and ISCCP data to assess clouds in the Hadley Centre, ECMWF and LMD atmospheric climate models, *Clim Dynam*, *17*(12), 905–922, doi:10.1007/s003820100157.

Wood, R., and C. S. Bretherton (2006), On the relationship between stratiform low cloud cover and lower-tropospheric stability, *J Climate*.

Yuan, T., L. Oreopoulos, M. Zelinka, and H. Yu (2016), Positive low cloud and dust feedbacks amplify tropical North Atlantic Multidecadal Oscillation, *Geoph. Res. Lett.*

Zelinka, M. D., C. Zhou, and S. A. Klein (2016), Insights from a refined decomposition of cloud feedbacks, *Geophys Res Lett*, *43*(17), 9259–9269, doi:10.1002/2016GL069917.

Zhang, R., and T. L. Delworth (2007), Impact of the Atlantic Multidecadal Oscillation on North Pacific climate variability, *Geophys Res Lett*, *34*(23), n/a–n/a, doi:10.1175/1520-0442(1996)009<1468:ICVOTN>2.0.CO;2.

Zhang, R., S. M. Kang, and I. M. Held (2010), Sensitivity of Climate Change Induced by the Weakening of the Atlantic Meridional Overturning Circulation to Cloud Feedback, *J Climate*, *23*(2), 378–389, doi:10.1175/2009JCLI3118.1.

Zhou, C., M. D. Zelinka, and S. A. Klein (2016), Impact of decadal cloud variations on the Earth's energy budget, *Nat Geosci*, *9*(12), 871–+, doi:10.1038/NGEO2828.

Zhou, Chen, Mark D. Zelinka, and Stephen A. Klein. "Analyzing the dependence of global cloud feedback on the spatial pattern of sea surface temperature change with a Green's function approach." *Journal of Advances in Modeling Earth Systems* 9, no. 5 (2017): 2174-2189

Acknowledgement:

This effort of T. Y. was supported by the National Aeronautics and Space Administration (NASA) Modeling Analysis and Prediction program (NNX13AM19G). HadCRUT4 data, ERSST data, MODIS level-3 data, and ISCCP corrected data are accessible from the following websites, respectively: https://crudata.uea.ac.uk/cru/data/temperature/, https://www.ncdc.noaa.gov/data-access/marineocean-data/extended-reconstructed-sea-surface-

temperature-ersst-v4 , and https://ladsweb.modaps.eosdis.nasa.gov, https://rda.ucar.edu/datasets/ds741.5/ . ERA-Interim reanalysis data can be ordered here https://www.ecmwf.int.